Robotica (2017) volume 35, pp. 2257–2277. © Cambridge University Press 2017
doi:10.1017/S0263574716000862

Kinematic effects of number of legs in 6-DOF UPS parallel mechanisms

Mohammad H. Abedinnasab†*, Farzam Farahmand‡, Bahram Tarvirdizadeh§, Hassan Zohoor¶ and Jaime Gallardo-Alvarado||

†*Department of Biomedical Engineering, Rowan University, Glassboro, New Jersey 08028, USA*
‡*School of Mechanical Engineering, Sharif University of Technology, Tehran, Iran; RCBTR, Tehran University of Medical Sciences, Tehran, Iran. E-mail: farahmand@sharif.edu*
§*Faculty of New Sciences and Technologies, University of Tehran, Tehran, Iran. E-mail: bahram@ut.ac.ir*
¶*Center of Excellence in Design, Robotics, and Automation, Sharif University of Technology, Tehran, Iran; Academy of Sciences of I.R.Iran, Tehran, Iran. E-mail: zohoor@sharif.ir*
||*Department of Mechanical Engineering, Instituto Tecnológico de Celaya, TNM, 38010 Celaya, GTO, México. E-mail: jaime.gallardo@itcelaya.edu.mx*

(Accepted December 20, 2016. First published online: January 31, 2017)

SUMMARY
In this paper, we study the kinematic effects of number of legs in 6-DOF UPS parallel manipulators. A group of 3-, 4-, and 6-legged mechanisms are evaluated in terms of the kinematic performance indices, workspace, singular configurations, and forward kinematic solutions. Results show that the optimum number of legs varies due to priorities in kinematic measures in different applications. The non-symmetric Wide-Open mechanism enjoys the largest workspace, while the well-known Gough–Stewart (3–3) platform retains the highest dexterity. Especially, the redundantly actuated 4-legged mechanism has several important advantages over its non-redundant counterparts and different architectures of Gough–Stewart platform. It has dramatically less singular configurations, a higher manipulability, and at the same time less sensitivity. It is also shown that the forward kinematic problem has 40, 16, and 1 solution(s), respectively for the 6-, 3-, and the 4-legged mechanisms. Superior capabilities of the 4-legged mechanism make it a perfect candidate to be used in more challenging 6-DOF applications in assembly, manufacturing, biomedical, and space technologies.

KEYWORDS: Redundant mechanisms; Gaugh–Stewart platform; Screw theory; Kinematic indices; Singularity analysis; Workspace.

1. Introduction

Mechanism design is one of the key issues in any robotic application.[1] Parallel Mechanisms (PMs) were first introduced by Gough and Whitehall[2] with an application in tire-testing equipment, followed by Stewart,[3] who designed a PM to be used in a flight simulator. The well-known Gough–Stewart platform is a 6-legged UPS PM with one linear actuator in each leg,[4] where U, P, and S denote universal, prismatic, and spherical joints, respectively. Although Gough–Stewart platform possesses notable load carrying characteristics, however these properties deteriorate rapidly with rotation of the moving platform. The very nature of the Gough–Stewart platform limits the orientational workspace to relatively small rotations, suffering from parallel singularities.[5,6]

With ever-increasing demand on the robot performance, redundant mechanisms, which are more capable and stiffer than their non-redundant counterparts, have attracted more attention in recent years.

* Corresponding author. E-mail: abedin@rowan.edu

Actuation redundancy eliminates singularity, enlarges the usable workspace, and greatly improves dexterity and manipulability.[7–12] Redundant actuation also increases the dynamical capability of a PM by increasing the load-carrying capacity and acceleration of motion, optimizing the load distribution among the actuators and reducing the energy consumption of the drivers.[13–16]

Using kinematic redundancy, several modifications of Gough-Stewart platform have been proposed to enhance its workspace. Wang and Gosselin[17] introduced a spatial 7-DOF kinematically redundant PM, by adding one additional revolute joint to the Gough–Stewart platform, which can be rotated around the vertical axis. Kotlarski et al.[18] introduced a kinematically redundant PM by adding an active prismatic joint to the Gough–Stewart platform. Gosselin and Schreiber[6] included kinematically redundant parallel legs in a Gough–Stewart platform, resulting in a 9-legged PM, to alleviate the orientational limitations due to singularities. In the above mentioned mechanisms, the number of legs and/or moving limbs, e.g. prismatic actuators, have been increased from that of the original Gough–Stewart platform, leading to the inescapable handle of moving mass inertias, reducing the dynamic performance due to lower achievable accelerations.

On the other hand, from the design point of view, by replacing the passive universal joints in the Gough–Stewart platform with active joints, the number of legs could be reduced from 6 to 3 or 4.[19,20] This makes the mechanism lighter, since the rotary actuators are resting on the fixed platform, which allows for higher accelerations to be achieved due to smaller inertial effects. The resultant 3-legged and 4-legged 6-DOF UPS mechanisms have two active actuators, one rotary and one prismatic, in each leg. It makes the 3-legged and 4-legged PMs to be non-redundant, and redundantly actuated mechanisms, respectively.

The purpose of the present study is to analyze and compare a group of 3-, 4-, and 6-legged 6-DOF UPS parallel manipulators, including the well-known architectures of the Gough–Stewart platform. The rest of the paper is organized as follows. In Section 2, the six 6-DOF redundant or non-redundant mechanisms which are to be compared are described. The inverse and forward kinematic analyses of the mechanisms are performed in Sections 3 and 4, respectively. Jacobian analysis is then performed in Section 5. In Section 6, the characteristics of the mechanisms are studied and compared in terms of the performance indices, workspace, singularity, and forward kinematic solutions. Two potential applications of the Wide-Open and 4-legged mechanisms (4L) are discussed in Section 7. Finally, a conclusion on the advantages of each proposed mechanism and their potential applications are provided in Section 8.

2. Mechanisms Description

The schematics of the 6-DOF non-redundant 3-legged and redundant 4L, as well as three architectures of the Gough–Stewart platform, are shown in Fig. 1. By replacing the passive universal joints in the Stewart mechanism with active joints, the number of legs could be reduced from 6 to 3 or 4. This change makes the mechanism to be lighter, since the rotary actuators are resting on the fixed platform, which causes higher accelerations to be available due to smaller inertial effects.

The basic non-redundant 3-legged mechanism has a symmetric structure.[19] The Wide-Open 3-legged mechanism has a similar structure but the legs are configured non-symmetrically on semicircles on the base and moving platforms. The redundant 4L, on the other hand, has a symmetric structure but includes an additional leg in comparison with the 3-legged systems.

Each leg in these systems is composed of three joints; universal, prismatic, and spherical (Figs. 2 and 3). A rotary actuator and a linear actuator are used to actuate each leg. The rotary actuators, whose shafts are attached to the lower parts of the linear actuators through the universal joints, are placed on the corners of the fixed platform.[20–22] The spherical joints connect the upper parts of the linear actuators to the moving platform.

As shown in the Fig. 3, coordinate $C_i(A_i,x_i,y_i,z_i)$ is assumed to be attached to the base platform with its x_i axis aligned with the rotary actuator in the x_i direction, and its z_i axis perpendicular to the fixed platform. x_i is rotated by γ_i from the X direction of fixed platform coordinate $A(O, X, Y, Z)$. The rotary actuators are located at the positions A_i (for $i = 1, 2, 3, 4$) of the base platform and each shaft is connected to the lower part of the linear actuators through a universal joint (Fig. 1). The upper parts of linear actuators are connected to the moving platform, B_i points, through spherical joints (Fig. 3).

Cartesian coordinates $A(O, x, y, z)$ and $B(P, u, v, w)$ represented by $\{A\}$ and $\{B\}$ are attached to the base and moving platforms, respectively. In Fig. 3, $\boldsymbol{s_i}$ represents the unit vector along the axes of ith rotary actuator and $\boldsymbol{d_i}$ is the vector along A_iB_i with the length of d_i. Assuming that each limb is

https://doi.org/10.1017/S0263574716000862 Published online by Cambridge University Press

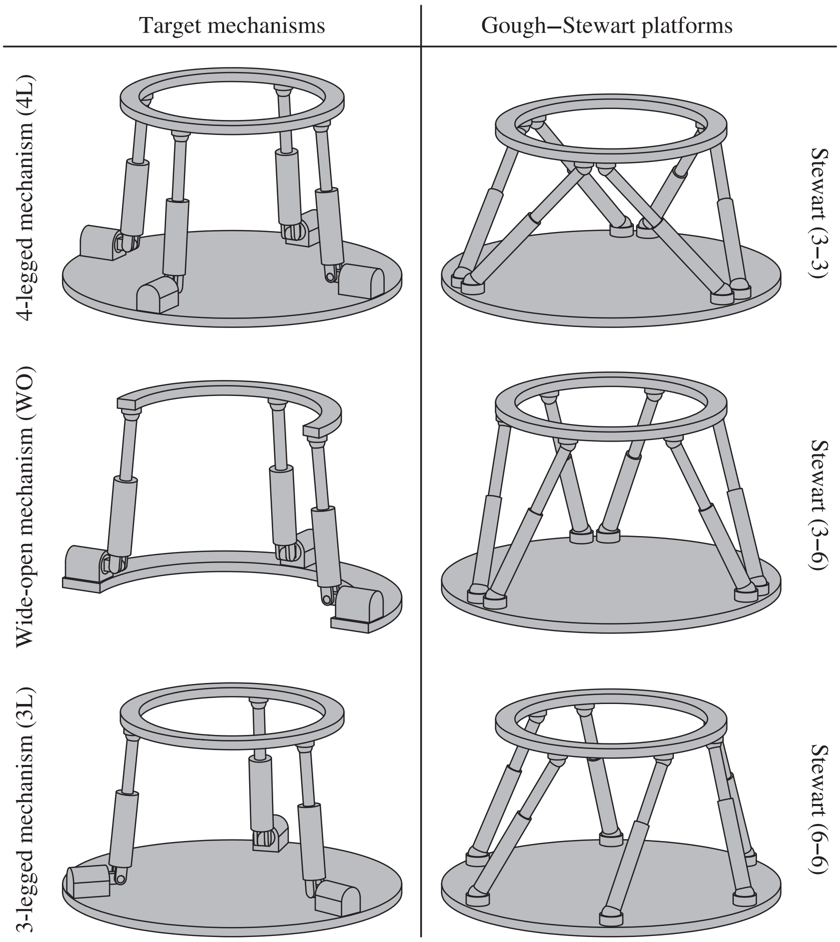

Fig. 1. Schematics of the 3- or 4-legged non-redundant and redundant mechanisms and Gough–Stewart platforms. Moving platform of all the mechanisms have six degrees of freedom. The mechanisms differ in the structure, number, and attachment positions of their legs. The 3- and 4-legged mechanisms have two active joints in each leg (one rotary and one linear), while the Gough–Stewart platforms have only a linear actuator in each leg.

connected to the fixed base by a universal joint, the orientation of ith limb with respect to the fixed base can be described by two successive rotations, rotation θ_i around the axis $\boldsymbol{s_i}$, followed by the rotation ψ_i around $\boldsymbol{n_i}$, which is itself perpendicular to both $\boldsymbol{d_i}$ and $\boldsymbol{s_i}$ (Fig. 3). It is to be noted that θ_i and d_i are active joints actuated by the rotary and linear actuators, respectively, while , ψ_i is an inactive joint.

3. Inverse Kinematic Analysis

Inverse kinematic analysis is a necessary step toward studying the parallel manipulators, which helps determining their applicability and performance characteristics. In this section, a general formulation for inverse kinematic analysis of all mechanisms under study is provided. The kinematic variables of the mechanisms are shown in Figs. 2–4.

Referring to Fig. 4, $\boldsymbol{a_i}$ and $\boldsymbol{b_i}$ represent OA_i and PB_i, respectively. We can express $\boldsymbol{b_i}$ in the moving coordinate $\{B\}$ as ${}^{\boldsymbol{B}}\boldsymbol{b_i} = PB_i)_B$. $\boldsymbol{a_i}$ and ${}^{\boldsymbol{B}}\boldsymbol{b_i}$ are constant vectors and are respectively equal to $\boldsymbol{a_i} = g[\cos\gamma_i \quad \sin\gamma_i \quad 0]^T$ and ${}^{\boldsymbol{B}}\boldsymbol{b_i} = h[\cos\gamma_i\ \sin\gamma_i\ 0]^T$, where g is the radius of the fixed platform, and h is that of the moving platform. The rotation matrix from $\{A\}$ to $\{B\}$, ${}^A_BR = [r_{ij}]$, can be expressed using Euler angles as

$$
{}^A_BR = \begin{bmatrix} c\alpha_2 c\alpha_3 & -c\alpha_2 s\alpha_3 & s\alpha_2 \\ c\alpha_3 s\alpha_2 s\alpha_1 + s\alpha_3 c\alpha_1 & -s\alpha_3 s\alpha_2 s\alpha_1 + c\alpha_3 c\alpha_1 & -c\alpha_2 s\alpha_1 \\ -c\alpha_3 s\alpha_2 c\alpha_1 + s\alpha_3 s\alpha_1 & s\alpha_3 s\alpha_2 c\alpha_1 + c\alpha_3 s\alpha_1 & c\alpha_2 c\alpha_1 \end{bmatrix}, \tag{1}
$$

https://doi.org/10.1017/S0263574716000862 Published online by Cambridge University Press

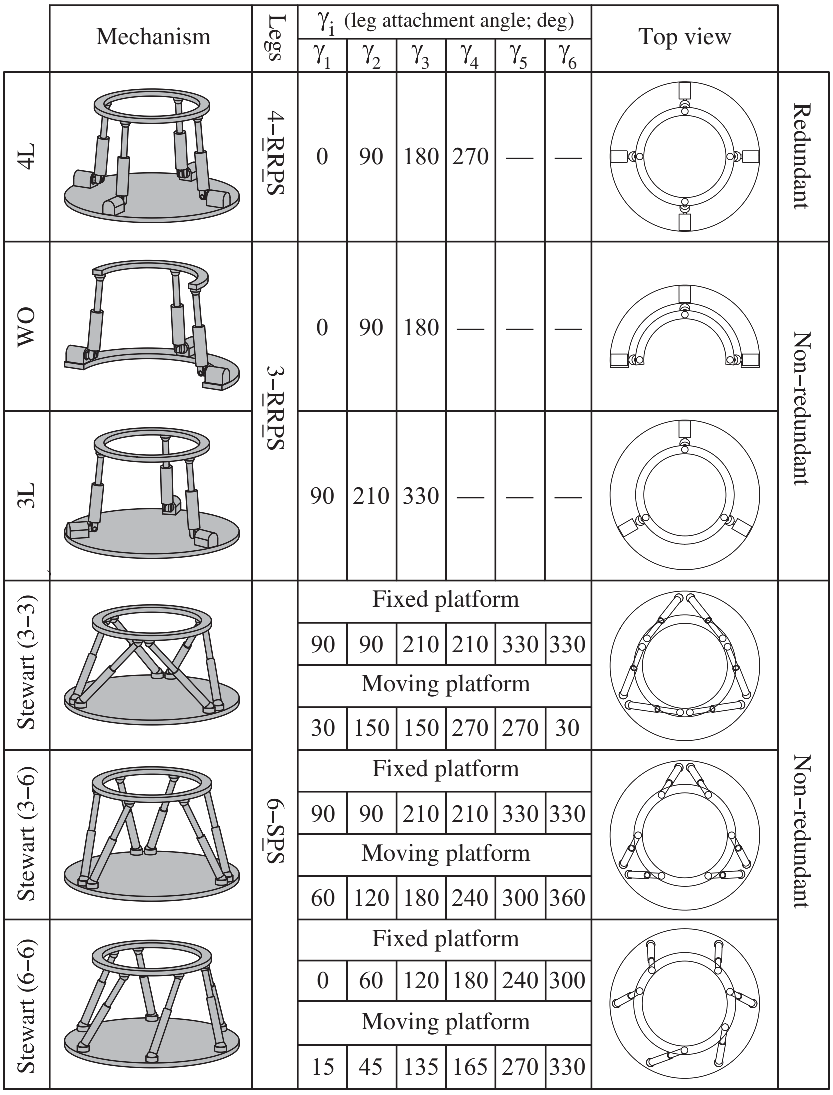

Fig. 2. Leg structure and attachment angles (γ_i's) of the 3- and 4-legged mechanisms and Gough–Stewart platforms. The leg attachment angles are the same for 4L, WO, and 3L mechanisms, but different for Gough–Stewart platforms. The 4L mechanism is the only redundantly actuated manipulator.

where $s\alpha_1 = \sin\alpha_1$, $c\alpha_1 = \cos\alpha_1$, and so on. α_1, α_2, and α_3 are three Euler angles defined according to the $x - y - z$ convention. Thus, the vector ${}^B\boldsymbol{b_i}$ would be expressed in the fixed frame $\{A\}$ as $\boldsymbol{b_i} = {}^A_B R\, {}^B\boldsymbol{b_i}$.

Let $\boldsymbol{p} = [\,x\ \ y\ \ z\,]^T$ denote the position vector of the center of the moving platform. Vector $\boldsymbol{d_i}$, which represents A_iB_i, can be written as

$$\boldsymbol{d_i} = \boldsymbol{p} + \boldsymbol{b_i} - \boldsymbol{a_i}. \tag{2}$$

Therefore, $\boldsymbol{d_i}$ can be expressed as

$$\boldsymbol{d_i} = \begin{bmatrix} x - x_i \\ y - y_i \\ z - z_i \end{bmatrix}, \tag{3}$$

https://doi.org/10.1017/S0263574716000862 Published online by Cambridge University Press

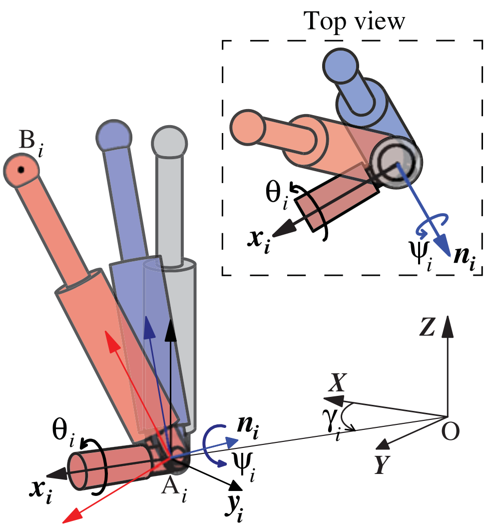

Fig. 3. Universal joint variables of ith leg are shown. θ_i is the active rotation around $\boldsymbol{x_i}$ axis, followed by the passive ψ_i rotation around $\boldsymbol{n_i}$ axis.

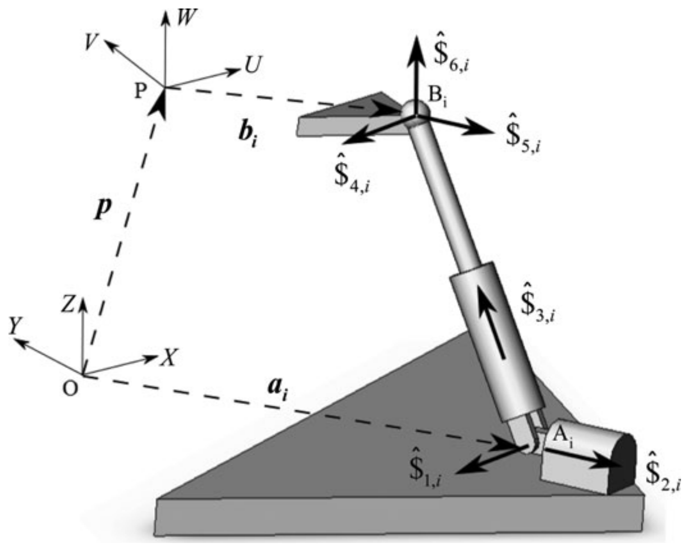

Fig. 4. Kinematic variables and infinitesimal screws in each leg.

and its Euclidean norm d_i, which is $|A_i B_i|$, can be expressed as

$$d_i = \sqrt{(x - x_i)^2 + (y - y_i)^2 + (z - z_i)^2}, \tag{4}$$

in which,

$$\begin{cases} x_i = -h\,(\cos\gamma_i\, r_{11} + \sin\gamma_i\, r_{21}) + g\cos\gamma_i, \\ y_i = -h\,(\cos\gamma_i\, r_{12} + \sin\gamma_i\, r_{22}) + g\sin\gamma_i, \\ z_i = -h\,(\cos\gamma_i\, r_{13} + \sin\gamma_i\, r_{23})\,. \end{cases} \tag{5}$$

Coordinates $C_i(A_i, x_i, y_i, z_i)$ are attached to the base platform with their x_i axes aligned with the rotary actuators in the $\boldsymbol{s_i}$ directions, with their z_i axes perpendicular to the fixed platform (Fig. 3).

https://doi.org/10.1017/S0263574716000862 Published online by Cambridge University Press

Thus, one can express vector $\boldsymbol{d_i}$ in $\{C_i\}$ as

$$^{C_i}\boldsymbol{d_i} = d_i \begin{bmatrix} \sin\psi_i \\ -\sin\theta_i \cos\psi_i \\ \cos\theta_i \cos\psi_i \end{bmatrix}. \tag{6}$$

From the geometry, it is clear that

$$\boldsymbol{d_i} = {}^{A}_{C_i}R\, ^{C_i}\boldsymbol{d_i}, \tag{7}$$

where ${}^{A}_{C_i}R$ is the rotation matrix from $\{C_i\}$ to $\{A\}$,

$${}^{A}_{C_i}R = \begin{bmatrix} \cos\gamma_i & -\sin\gamma_i & 0 \\ \sin\gamma_i & \cos\gamma_i & 0 \\ 0 & 0 & 1 \end{bmatrix}. \tag{8}$$

By replacing Eqs. (6) and (8) into Eq. (7), and using Eq. (3), ψ_i and θ_i can be calculated as follows:

$$\psi_i = \sin^{-1}\left(\frac{\cos\gamma_i(x - x_i) + \sin\gamma_i(y - y_i)}{d_i}\right), \tag{9}$$

and

$$\theta_i = \sin^{-1}\left(\frac{\sin\gamma_i(x - x_i) - \cos\gamma_i(y - y_i)}{d_i \cos\psi_i}\right). \tag{10}$$

Finally, the active joint variables for the 4L, WO, and 3L mechanisms are d_i and θ_i which are shown in Eqs. (4) and (10), respectively. Active joints in Gough–Stewart platform are only d_i's, Eq. (4).

4. Forward Kinematic Analysis

The forward kinematic problem of Gough–Stewart platform has been shown to have a large number of 40 solutions.[23–25] In this section, we derive the equations which solve the forward kinematic problem of the proposed 3-legged, Wide-Open, and 4-legged parallel manipulators. The forward displacement analysis consists of finding all the reachable poses of the moving platform as observed from the base for a given set of active joints θ_i and d_i. This problem is approached here by considering the fact that the pose of any rigid body can be specified by the coordinates of any three points attached to it. Thus, the pose of the moving platform with respect to the fixed platform can be fully determined using the coordinates of points B_i (for $i = 1, 2, 3$) with respect to the fixed reference frame $\{A\}$, which is denoted as $\boldsymbol{r_i}$, where

$$\boldsymbol{r_i} = \boldsymbol{a_i} + {}^{A}_{C_i}R\, ^{C_i}\boldsymbol{d_i}. \tag{11}$$

By replacing $\boldsymbol{a_i}$, ${}^{A}_{C_i}R$, and $^{C_i}\boldsymbol{d_i}$ from Section 3 into Eq. (11), $\boldsymbol{r_i}$ is obtained as

$$\boldsymbol{r_i} = d_i \begin{bmatrix} \cos\gamma_i \sin\psi_i + \sin\gamma_i \sin\theta_i \cos\psi_i \\ \sin\gamma_i \sin\psi_i - \cos\gamma_i \sin\theta_i \cos\psi_i \\ \cos\theta_i \cos\psi_i \end{bmatrix} + g \begin{bmatrix} \cos\gamma_i \\ \sin\gamma_i \\ 0 \end{bmatrix}. \tag{12}$$

Using the geometry of the moving platform and the distance between points B_i, the following equations are readily obtained:

$$(\boldsymbol{r_1} - \boldsymbol{r_2})^T \cdot (\boldsymbol{r_1} - \boldsymbol{r_2}) = |B_1 B_2|^2,$$
$$(\boldsymbol{r_1} - \boldsymbol{r_3})^T \cdot (\boldsymbol{r_1} - \boldsymbol{r_3}) = |B_1 B_3|^2, \quad (13)$$
$$(\boldsymbol{r_2} - \boldsymbol{r_3})^T \cdot (\boldsymbol{r_2} - \boldsymbol{r_3}) = |B_2 B_3|^2,$$

where $|B_1 B_2|$, $|B_1 B_3|$, and $|B_2 B_3|$ are respectively $\sqrt{2}h$, $2h$, and $\sqrt{2}h$ for Wide-Open mechanism, while they are all equal to $\sqrt{3}h$ for the 3-legged one.

After replacing $\boldsymbol{r_i}$'s in Eq. (13) with those in Eq. (11), the only unknown variables would be the inactive ψ_i joints. Therefore, one can solve a set of three equations (13) with three unknowns ψ_i's. Using the tangent half-angle formula, $\sin\psi_i$ and $\cos\psi_i$ can be respectively replaced by $2t_i/(1+t_i^2)$ and $(1-t_i^2)/(1+t_i^2)$, where $t_i = \tan(\psi_i/2)$. Using the Bezout's theorem,[26] it can be shown that Eqs. (13) have 16 solutions, at most.[27] It is incredibly less than the 40 solutions of forward kinematics in Gough–Stewart platform.[23–25]

For the redundant 4L, auxiliary equations can be used as

$$(\boldsymbol{r_i} - \boldsymbol{r_4})^T \cdot (\boldsymbol{r_i} - \boldsymbol{r_4}) = |B_i B_4|^2, \quad (14)$$

in which $i = 1, 2, 3$. It is to be noted that $|B_1 B_4|$, $|B_2 B_4|$, and $|B_3 B_4|$ are respectively $\sqrt{2}h$, $2h$, and $\sqrt{2}h$. In Section 6.4, the forward kinematic solutions of the proposed mechanisms are evaluated and compared through a numerical example.

5. Jacobian Analysis Using Screw Theory

Jacobian matrix is a common asset for analyzing the singularity in a mechanism.[5] In this section, the jacobian analysis of the proposed PMs are approached by using the theory of screws (see ref. [21,28–30]). Zhao *et al.*[31] have proposed an intuitive geometrical approach to obtain the reciprocal screws in PM. In what follows, we have used their approach in conducting the reciprocal screws in the mechanisms.

The joint velocity vector of the redundant 4L mechanism, $\dot{\boldsymbol{q}}^{4L}$, is an 8×1 vector:

$$\dot{\boldsymbol{q}}^{4L} = [\,\dot{\theta}_1\ \dot{\theta}_2\ \ \dot{\theta}_3\ \dot{\theta}_4\ \dot{d}_1\ \ \dot{d}_2\ \dot{d}_3\ \dot{d}_4\,]^T, \quad (15)$$

in which $\dot{\theta}_i$ and $\dot{d}_i$ are the angular and linear velocities of the rotary and linear actuators, respectively. However, joint velocity vector in the non-redundant WO and 3L mechanisms, $\dot{\boldsymbol{q}}^{WO}$ and $\dot{\boldsymbol{q}}^{3L}$, are 6×1 vectors:

$$\dot{\boldsymbol{q}}^{WO} = \dot{\boldsymbol{q}}^{3L} = [\,\dot{\theta}_1\ \dot{\theta}_2\ \dot{\theta}_3\ \dot{d}_1\ \dot{d}_2\ \dot{d}_3\,]^T. \quad (16)$$

Finally, joint velocity vector of the Gough–Stewart platforms are

$$\dot{\boldsymbol{q}}^{St.} = [\,\dot{d}_1\ \dot{d}_2\ \dot{d}_3\ \dot{d}_4\ \dot{d}_5\ \dot{d}_6\,]^T. \quad (17)$$

The linear and angular velocities of the moving platform are defined to be $\boldsymbol{v}$ and ω, respectively. Thus, $\dot{\boldsymbol{x}}$ can be written as a 6×1 velocity vector:

$$\dot{\boldsymbol{x}} = [\boldsymbol{v}^T \qquad \omega^T]. \quad (18)$$

Jacobian matrices relate $\dot{\boldsymbol{q}}$ and $\dot{\boldsymbol{x}}$ as follows:

$$J_x \dot{\boldsymbol{x}} = J_q \dot{\boldsymbol{q}}, \quad (19)$$

https://doi.org/10.1017/S0263574716000862 Published online by Cambridge University Press

where J_x and J_q are forward and inverse jacobian matrices, respectively. By defining $J = J_q^{-1} J_x$, we rewrite Eq. (19) as

$$\dot{\boldsymbol{q}} = J\dot{\boldsymbol{x}}. \tag{20}$$

The concept of reciprocal screws is applied to derive J_x and J_q.[32,33] The reference frame of the screws is point P of the moving platform. Figure 4 shows the kinematic chain of each leg, where universal joints are replaced by intersection of two unit screws, $\hat{\$}_1$ and $\hat{\$}_2$. $\hat{\$}_1 = [{}^{\boldsymbol{s}_{1,i}}_{(\boldsymbol{b}_i - \boldsymbol{d}_i)\times \boldsymbol{s}_{1,i}}]$ and $\hat{\$}_2 = [{}^{\boldsymbol{s}_{2,i}}_{(\boldsymbol{b}_i - \boldsymbol{d}_i)\times \boldsymbol{s}_{2,i}}]$, where $\boldsymbol{s}_{1,i}$ and $\boldsymbol{s}_{2,i}$ are unit vectors. Spherical joints in each leg are replaced by intersection of three unit screws, $\hat{\$}_4$, $\hat{\$}_5$, and $\hat{\$}_6$. $\hat{\$}_4 = [{}^{\boldsymbol{s}_{4,i}}_{\boldsymbol{b}_i \times \boldsymbol{s}_{4,i}}]$, $\hat{\$}_5 = [{}^{\boldsymbol{s}_{5,i}}_{\boldsymbol{b}_i \times \boldsymbol{s}_{5,i}}]$, and $\hat{\$}_6 = [{}^{\boldsymbol{s}_{6,i}}_{\boldsymbol{b}_i \times \boldsymbol{s}_{6,i}}]$, where $\boldsymbol{s}_{4,i} = \boldsymbol{s}_{1,i}$. $\boldsymbol{s}_{6,i}$ is the unit vector along the linear actuator, and $\boldsymbol{s}_{5,i} = \boldsymbol{s}_{6,i} \times \boldsymbol{s}_{4,i}$. $\hat{\$}_3 = [{}^{0}_{\boldsymbol{s}_{3,i}}]$ explains the prismatic joint. It is to be noted that $\boldsymbol{s}_{3,i} = \boldsymbol{s}_{6,i}$. Each leg can be assumed as an open-loop chain to express the instant twist of the moving platform by means of the joint screws:

$$\hat{\$}_P = \dot{\psi}_i \hat{\$}_{1,i} + \dot{\theta}_i \hat{\$}_{2,i} + \dot{d}_i \hat{\$}_{3,i} + \dot{\phi}_{1,i} \hat{\$}_{4,i} + \dot{\phi}_{2,i} \hat{\$}_{5,i} + \dot{\phi}_{3,i} \hat{\$}_{6,i}. \tag{21}$$

By taking the orthogonal product of both sides of Eq. (21) with reciprocal screw $\hat{\$}_{r1,i} = [{}^{\boldsymbol{s}_{3,i}}_{\boldsymbol{b}_i \times \boldsymbol{s}_{3,i}}]$, one can eliminate the inactive joints and rotary actuator which yields Eq. (22):

$$\left[\frac{\boldsymbol{d}_i{}^T}{d_i} \quad \frac{(\boldsymbol{b}_i \times \boldsymbol{d}_i)^T}{d_i} \right] \dot{\boldsymbol{x}} = \dot{d}_i. \tag{22}$$

Similarly, if one takes the orthogonal product of both sides of Eq. (21) with reciprocal screw $\hat{\$}_{r6,i} = \begin{bmatrix} \frac{\boldsymbol{s}_i \times \boldsymbol{d}_i}{d_i \cos\psi_i} \\ \boldsymbol{b}_i \times \frac{\boldsymbol{s}_i \times \boldsymbol{d}_i}{d_i \cos\psi_i} \end{bmatrix}$ the resultant is as follows:

$$\left[\left(\frac{\boldsymbol{s}_i \times \boldsymbol{d}_i}{d_i \cos\psi_i}\right)^T \quad \left(\boldsymbol{b}_i \times \frac{\boldsymbol{s}_i \times \boldsymbol{d}_i}{d_i \cos\psi_i}\right)^T \right] \dot{\boldsymbol{x}} = d_i \cos\psi_i \dot{\theta}_i. \tag{23}$$

Note that in Eq. (23), $|\boldsymbol{s}_i \times \boldsymbol{d}_i| = d_i \cos\psi_i$.

Finally, using Eqs. (22) and (23), jacobian matrices J_x^{4L} and J_q^{4L} are expressed as

$$J_x^{4L} = \begin{bmatrix} (\boldsymbol{s}_1 \times \boldsymbol{d}_1)^T & (\boldsymbol{b}_1 \times (\boldsymbol{s}_1 \times \boldsymbol{d}_1))^T \\ (\boldsymbol{s}_2 \times \boldsymbol{d}_2)^T & (\boldsymbol{b}_2 \times (\boldsymbol{s}_2 \times \boldsymbol{d}_2))^T \\ (\boldsymbol{s}_3 \times \boldsymbol{d}_3)^T & (\boldsymbol{b}_3 \times (\boldsymbol{s}_3 \times \boldsymbol{d}_3))^T \\ (\boldsymbol{s}_4 \times \boldsymbol{d}_4)^T & (\boldsymbol{b}_4 \times (\boldsymbol{s}_4 \times \boldsymbol{d}_4))^T \\ \boldsymbol{d}_1{}^T & (\boldsymbol{b}_1 \times \boldsymbol{d}_1)^T \\ \boldsymbol{d}_2{}^T & (\boldsymbol{b}_2 \times \boldsymbol{d}_2)^T \\ \boldsymbol{d}_3{}^T & (\boldsymbol{b}_3 \times \boldsymbol{d}_3)^T \\ \boldsymbol{d}_4{}^T & (\boldsymbol{b}_4 \times \boldsymbol{d}_4)^T \end{bmatrix}, \tag{24}$$

and

$$J_q^{4L} = diag(d_1^2 \cos^2\psi_1, d_2^2 \cos^2\psi_2, d_3^2 \cos^2\psi_3, d_4^2 \cos^2\psi_4, d_1, d_2, d_3, d_4). \tag{25}$$

https://doi.org/10.1017/S0263574716000862 Published online by Cambridge University Press

Similarly, forward and inverse jacobian matrices for non-redundant mechanisms can be expressed as

$$J_x^{WO} = J_x^{3L} = \begin{bmatrix} (\boldsymbol{s}_1 \times \boldsymbol{d}_1)^T & (\boldsymbol{b}_1 \times (\boldsymbol{s}_1 \times \boldsymbol{d}_1))^T \\ (\boldsymbol{s}_2 \times \boldsymbol{d}_2)^T & (\boldsymbol{b}_2 \times (\boldsymbol{s}_2 \times \boldsymbol{d}_2))^T \\ (\boldsymbol{s}_3 \times \boldsymbol{d}_3)^T & (\boldsymbol{b}_3 \times (\boldsymbol{s}_3 \times \boldsymbol{d}_3))^T \\ \boldsymbol{d}_1{}^T & (\boldsymbol{b}_1 \times \boldsymbol{d}_1)^T \\ \boldsymbol{d}_2{}^T & (\boldsymbol{b}_2 \times \boldsymbol{d}_2)^T \\ \boldsymbol{d}_3{}^T & (\boldsymbol{b}_3 \times \boldsymbol{d}_3)^T \end{bmatrix}, \tag{26}$$

and

$$J_q^{WO} = J_q^{3L} = diag(d_1^2\cos^2\psi_1, d_2^2\cos^2\psi_2, d_3^2\cos^2\psi_3, d_1, d_2, d_3). \tag{27}$$

Also for the Stewart platforms we will have

$$J_x^{St.} = \begin{bmatrix} \boldsymbol{d}_1{}^T & (\boldsymbol{b}_1 \times \boldsymbol{d}_1)^T \\ \boldsymbol{d}_2{}^T & (\boldsymbol{b}_2 \times \boldsymbol{d}_2)^T \\ \boldsymbol{d}_3{}^T & (\boldsymbol{b}_3 \times \boldsymbol{d}_3)^T \\ \boldsymbol{d}_4{}^T & (\boldsymbol{b}_4 \times \boldsymbol{d}_4)^T \\ \boldsymbol{d}_5{}^T & (\boldsymbol{b}_5 \times \boldsymbol{d}_5)^T \\ \boldsymbol{d}_6{}^T & (\boldsymbol{b}_6 \times \boldsymbol{d}_6)^T \end{bmatrix}, \tag{28}$$

and

$$J_q^{St.} = diag(d_1, d_2, d_3, d_4, d_5, d_6). \tag{29}$$

Based on the existence of the two jacobian matrices above, the mechanism is at a singular configuration when the determinant of either J_x or J_q is either zero or infinity.[19,21] We will analyze the derived jacobian matrices in Section 6.

6. Results and Discussion

In order to investigate the performance of the mechanisms under study, the responses of the mechanisms are analyzed and compared in several different aspects, including the kinematic indices, workspace, and singularity analysis.

6.1. Kinematic indices

Several indices have been proposed to evaluate the performance of a manipulator. The performance indices are usually based on the determinant, norms, singular values, and eigenvalues of the jacobian matrix. These indices have physical interpretations, they give us more insight into the mechanisms performance in various aspects, and they are also useful for control and optimization purposes.

To compare the kinematic performance of the six mechanisms, we consider a number of different performance indices, namely *Manipulability Index*,[34,35] *Dexterity Index*,[36] and *Translational/Rotational Sensitivity Index*.[37] Consider the mechanisms with $g = 0.156$ (m) and $h = 0.102$ (m), where g and h are the radii of the fixed and moving platforms, respectively. Figure 5 shows the selected plane $z = 0.3$ (m), in which the indices measurements have been taken place at the center of moving platform, P. The results illustrated in Fig. 6 show how performance indices vary on the plane $z = 0.3$ (m) within the $[-0.4, 0.4] \times [-0.4, 0.4]$ (m^2) area.

Figure 6 indicates that the 4L has the highest manipulability index compared to the other mechanisms. It means that adding one leg to the symmetric or Wide-Open 3-legged mechanism can significantly improve the manipulability of the mechanism. Figure 6 also shows that compared to the other mechanisms under study, Stewart (3–3) and then the 4L have the highest dexterity indices.

Table I. Comparison of the global performance indices of the six mechanisms under study in the entire workspace.

	The higher, the better		The lower, the better	
Mechanism	Manipulability[35]	Dexterity[36]	Trans. sens.[37]	Rot. sens.[37]
4L	**0.027**	0.095	**0.510**	**8.424**
WO	0.015	0.059	0.602	10.629
3L	0.024	0.078	0.584	9.152
Stewart (3–3)	0.024	**0.113**	2.854	20.249
Stewart (3–6)	0.014	0.073	4.614	35.032
Stewart (6–6)	0.003	0.018	6.005	62.557

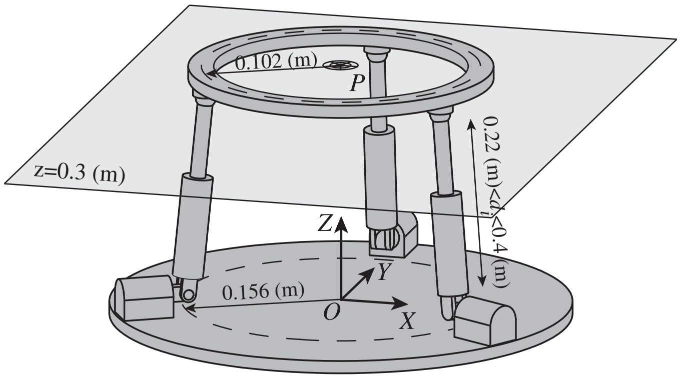

Fig. 5. Mechanical constraints of the legs, dimensions of the mechanisms, and illustration of the constant z plane in the numerical solutions.

In the next step of performance comparison of manipulators, translational and rotational sensitivities of the mechanisms of interest are compared. As it is shown in the figure, the 4L has less translational sensitivity index by far. Moreover, it is clear that similar to the displacement sensitivity, the rotational sensitivity of the 4L is less than the other mechanisms.

To compare the kinematic performance of manipulators over the entire workspace, the Global Performance Index (GPI) can be evaluated as[38]

$$GPI = \frac{\int_W PI \, dW}{\int_W dW}, \tag{30}$$

which is the average value of the local Performance index (PI) over the Workspace (W). The values of GPI for Manipulability, Dexterity, Displacement Sensitivity, and Rotation Sensitivity indices are calculated and the results are listed in Table I.

Table I shows that the 4L has a better global manipulability within the selected workspace, which explicitly indicates a better ability for transmitting a certain velocity to its end-effector. As it is seen from Table I, the Stewart (3–3) platform has the highest global dexterity compared to other mechanisms with the 4L being at the second position. This reveals that the Stewart (3–3) platform and the 4L have a better kinematic accuracy. Also, by comparing the values of translational and rotational sensitivities, it is obvious the 4L is an appropriate candidate for industrial applications due to its lower sensitivity. In general, based on the results shown in Table I, the 4L is found to have a better kinematic performance in comparison with the other mechanism under study.

6.2. Workspace

The workspaces of the mechanisms under study within a cubic space were determined in terms of their reachable points. The minimum and maximum lengths of the legs are set to be 0.22 (m) and 0.4 (m), respectively (see Fig. 5). The other physical constraint is the rotation limit of

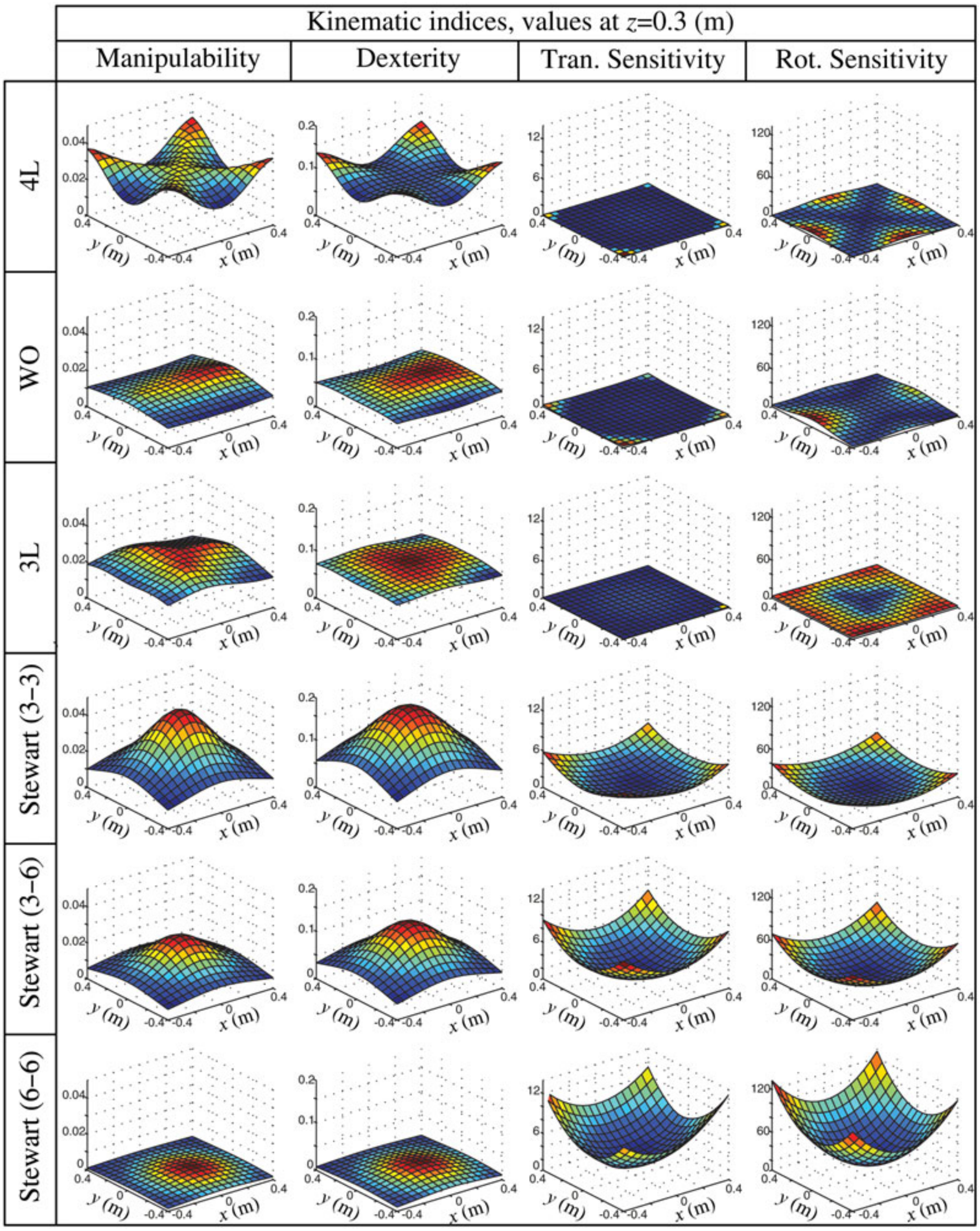

Fig. 6. Kinematic performance indices, namely *Manipulability Index*,[34,35] *Dexterity Index*,[36] and *Translational/Rotational Sensitivity Index*,[37] of the six mechanisms under study at $z = 0.3$ (m).

spherical joints which is considered to be $\pm 50^{\circ}$. By assuming a cubic with 0.6 (m) length, 0.6 (m) width, and 0.18 (m) height located 0.31 (m) above the base platform, we are interested in determining the space volume where each mechanism can successfully reach the locations within this cube.

The results, illustrated in Fig. 7, indicate that the 3-legged and 4L have much larger workspaces in comparison with the (3–6) and (3–3) Stewart Platforms. This is due to the fact that in the 6-legged Stewart-like UPS mechanisms, the workspace is constructed by intersection of six spheres. However, in the 3- and 4-legged UPS mechanism, the workspace is constructed by intersection of only three or four spheres. Assuming similar dimensions for the two mechanisms, a larger workspace would not be unexpected for the 3- and 4-legged mechanisms.

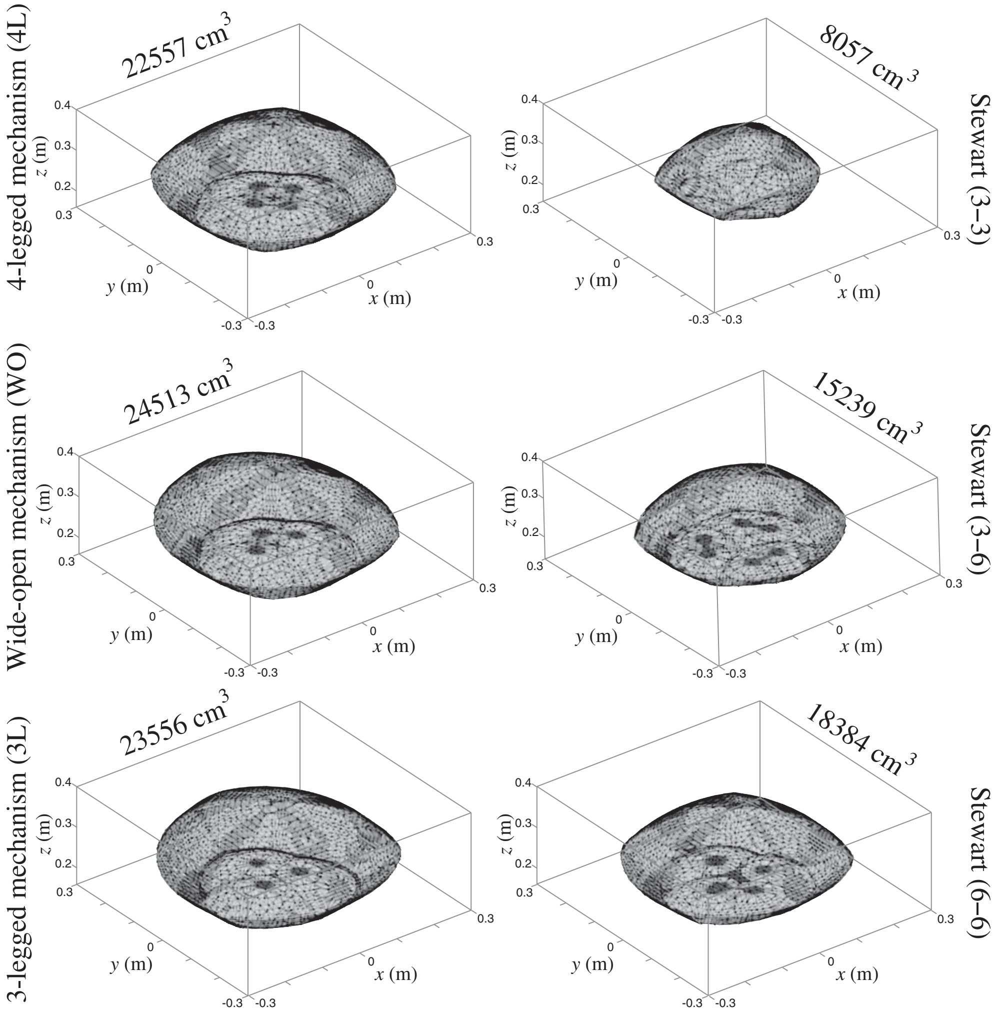

Fig. 7. Workspaces of the mechanisms under study.

On the other hand, as can be seen in the figure, adding one leg to the basic 3-legged mechanism reduces the workspace by about 5%. However, the quality of the workspaces is not the same. Although the redundant mechanism has a relatively smaller workspace, it has much less singular configurations within this space in comparison with the non-redundant mechanism, as well as lower actuator forces and torques.

6.3. Singularity

Singularity of parallel manipulators implies significantly more complicated problems compared to serial mechanisms. Several types of workspace can be considered to determine the singular configurations within. For example, the 3D constant orientation workspace, which describes all possible locations of an arbitrary point P in the moving system with a constant orientation of the moving platform, the reachable workspace (all locations that can be reached by P), the orientation workspace (all possible orientations of the end-effector around P for a given position), or the inclusive orientation workspace (all locations that can be reached by the origin of the end-effector with every orientation in a given set).[20]

Here, we used the inclusive orientation workspace, where for every position in a fixed surface, the moving platform is rotated in every possible orientation, to determine if a configuration is singular or not. After trials and errors, it is found that for a better determination of the singular configurations, the roll-pitch-yaw rotation about the global coordinate provides the most critical set of rotations compared to the other alternatives such as the reduced Euler rotations.

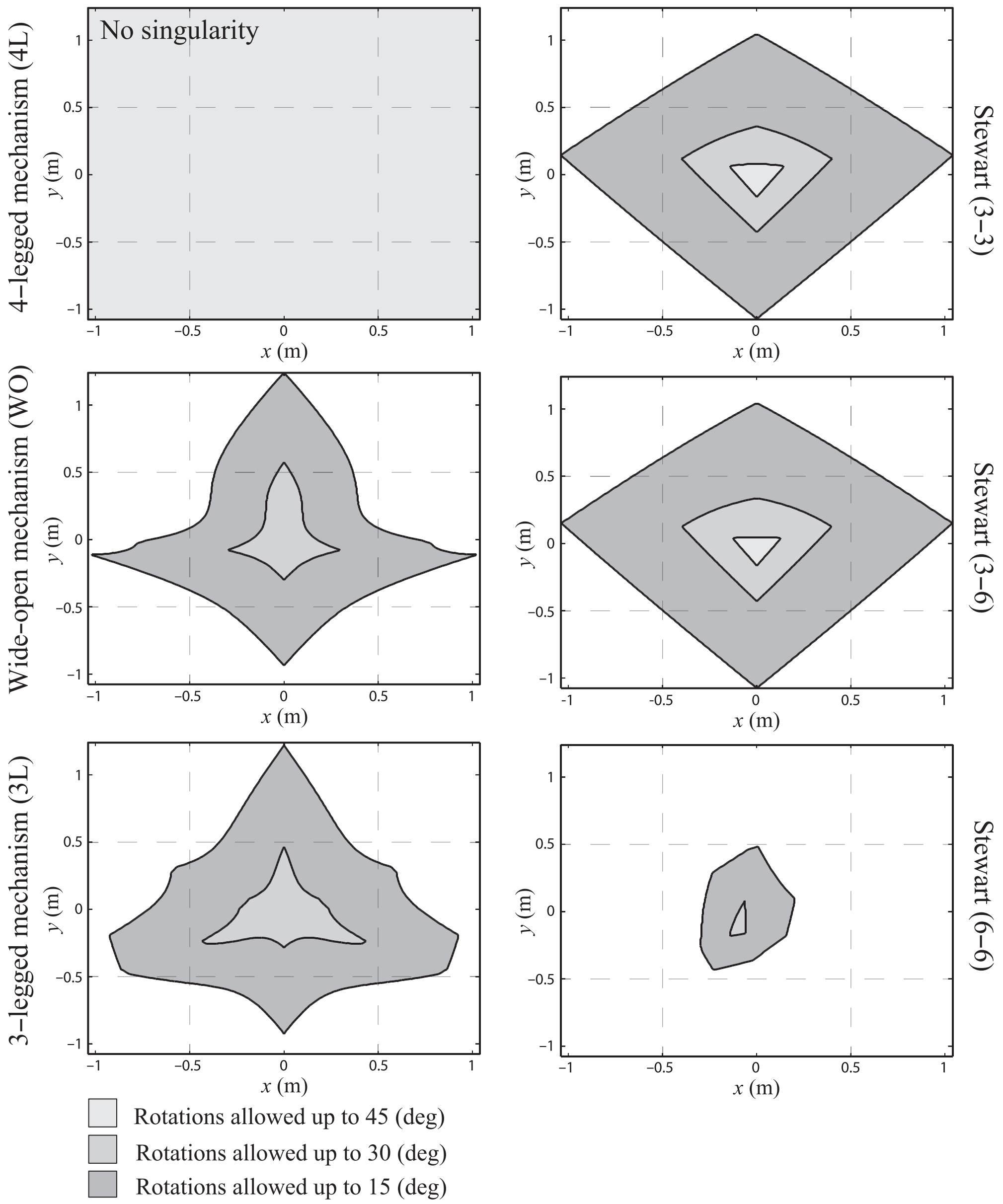

Fig. 8. The results of the singularity analysis in Z plane for the mechanisms under study.

To illustrate the positive effects of redundancy on eliminating the singular configurations, a Jacobian analysis was performed in planes with different orientations in the workspace. Figure 8 illustrates the results obtained for the mechanisms under study at the plane $z = 0.3$ (m). The moving platforms were rotated simultaneously in three different directions according to the roll-pitch-yaw Euler angles discussed above. For each position, if the mechanism did not encounter any singular configuration after 45° rotation, it was represented by light gray. If there was any singular configuration after 30° rotation but not after 15° rotation, it was shown with dark gray. Finally, if the singular configuration occurred in the first 15° rotation, it was represented by black.

As seen from Fig. 8, for the 3-legged mechanisms, there are singular configurations in most of the regions (dark gray and gray regions). However, for the redundant 4L, there is no singular points in the z plane. These results approve the great effect of a simple redundancy; namely, the addition of a leg to the 3-legged mechanism in removing lots of singular configurations.

https://doi.org/10.1017/S0263574716000862 Published online by Cambridge University Press

Table II. Forward kinematic solution of the 4-legged mechanism. The data correspond to the position of the center of the moving platform.

Solution	x (m)	y (m)	z (m)
1	0.1000	0.2000	0.3000

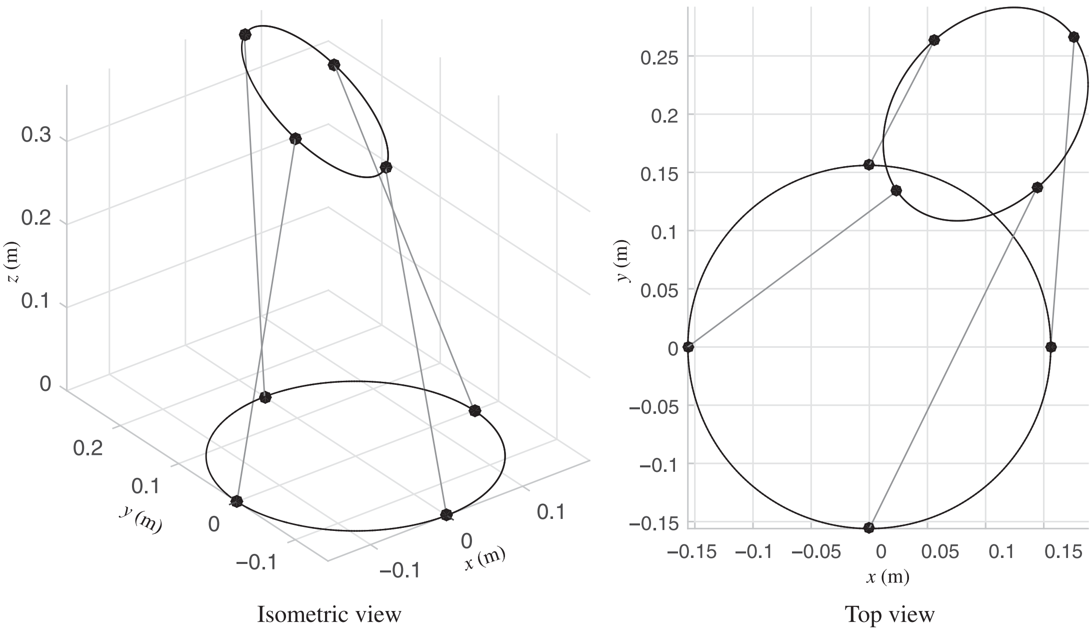

Fig. 9. Schematics of the forward kinematic solution of the 4-legged mechanism. Both isometric and top views of the mechanism are illustrated. Four legs connect the moving platform to the fixed one.

6.4. Forward kinematic solutions

In this section, we evaluate and compare the solutions of the forward kinematic problem of the proposed mechanisms through a numerical example. Consider the center of the moving platform is located at [0.1, 0.2, 0.3] (m), and the orientation of the moving platform is defined by three successive Euler angles of $\pi/6$, $\pi/6$, and $\pi/6$ in $x - y - z$ convention. Using the inverse kinematic equations, i.e. Eqs. (4) and (10), the values for active joints d_i's and θ_i's are readily computed using the position and orientation of the moving platform. It is to be noted that the only active joints in Gough–Stewart platforms are d_i's. After deriving the values of the active joints for all the proposed mechanisms, we attempt regenerating the location of the moving platform using the forward kinematic formulations presented in Section 4. For brevity, only the results of the 4-legged, 3-legged, and Stewart-6–6 mechanisms are presented and discussed.

6.4.1. The 4-legged mechanism. The solution of the forward kinematic problem for the 4L is presented in Table II. The data in the table correspond to the position of the center of the moving platform. Thanks to the redundancy, there is only one solution for the forward kinematic problem which matches the desired position of the moving platform. It means the redundancy has reduced the 16 potential number of solutions to only one. Schematic representation of the solution is shown in Fig. 9 with four links connecting the moving platform to the fixed one. Isometric and top views of the mechanism are shown in the figure.

6.4.2. The 3-legged mechanism. The solutions of the forward kinematic problem for the 3-legged mechanism are presented in Table III. The data in the table correspond to the position of the center of the moving platform. As seen in the table, the forward kinematic problem has 16 solutions. The first four solutions are real, and the rest are complex. Therefore, beside the desired first solution, there are

https://doi.org/10.1017/S0263574716000862 Published online by Cambridge University Press

Table III. Forward kinematic solutions of the 3-legged mechanism. The data correspond to the position of the center of the moving platform.

Solution	x (m)	y (m)	z (m)
1	0.1000	0.2000	0.3000
2	0.0350	0.2060	0.2853
3	−0.0883	−0.2094	−0.2953
4	−0.1353	−0.1553	−0.2783
5	$-0.1018 + 0.0737\,i$	$-0.0276 - 0.1200\,i$	$-0.3230 - 0.0399\,i$
6	$-0.1018 - 0.0737\,i$	$-0.0276 + 0.1200\,i$	$-0.3230 + 0.0399\,i$
7	$0.1658 + 0.0051\,i$	$0.1665 - 0.0702\,i$	$0.2902 - 0.0039\,i$
8	$0.1658 - 0.0051\,i$	$0.1665 + 0.0702\,i$	$0.2902 + 0.0039\,i$
9	$-0.1423 + 0.0374\,i$	$-0.1713 - 0.0044\,i$	$-0.2568 + 0.0073\,i$
10	$-0.1423 - 0.0374\,i$	$-0.1713 + 0.0044\,i$	$-0.2568 - 0.0073\,i$
11	$0.0560 + 0.0225\,i$	$0.2162 - 0.0409\,i$	$0.2563 - 0.0003\,i$
12	$0.0560 - 0.0225\,i$	$0.2162 + 0.0409\,i$	$0.2563 + 0.0003\,i$
13	$-0.0458 + 0.0477\,i$	$-0.2357 + 0.0213\,i$	$-0.2820 + 0.0078\,i$
14	$-0.0458 - 0.0477\,i$	$-0.2357 - 0.0213\,i$	$-0.2820 - 0.0078\,i$
15	$-0.0515 + 0.1311\,i$	$0.1074 + 0.0022\,i$	$0.3178 + 0.0402\,i$
16	$-0.0515 - 0.1311\,i$	$0.1074 - 0.0022\,i$	$0.3178 - 0.0402\,i$

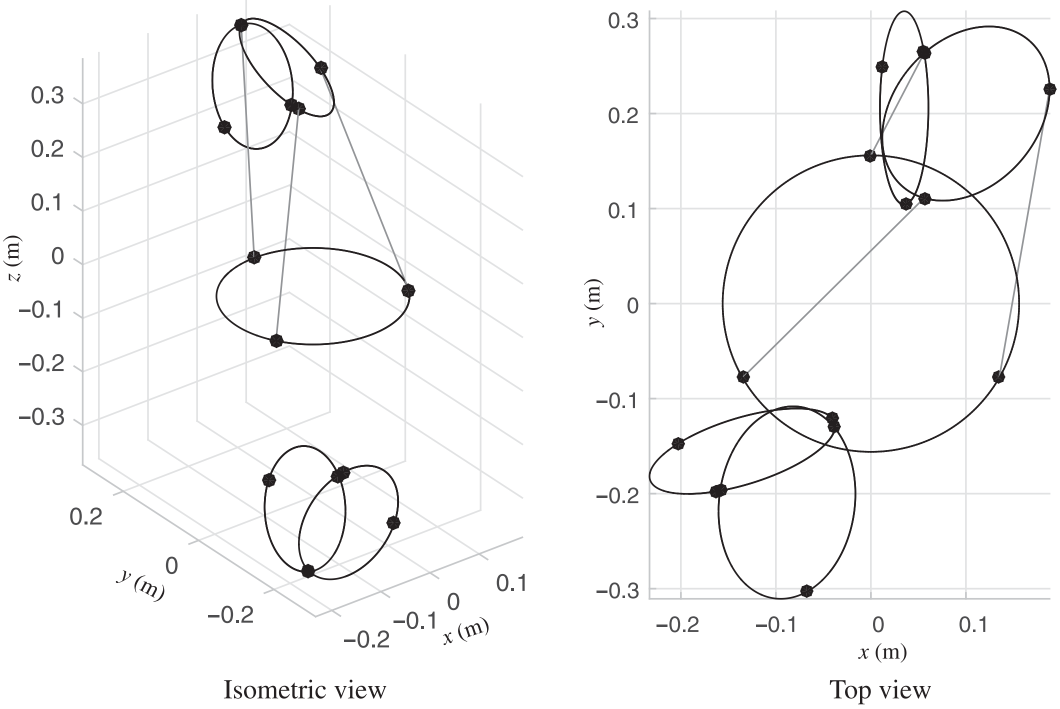

Fig. 10. Schematics of the real solutions of the forward kinematic problem of the 3-legged mechanism. Both isometric and top views of the solutions are illustrated. Three legs connect the moving platform to the fixed one.

three more possible poses for the moving platform which satisfy the forward kinematic equations. Schematic representations of the four real solutions are shown in Fig. 10 with three legs connecting the moving platform to the fixed one. Isometric and top views of the mechanism are shown in the figure.

6.4.3. The Stewart-6–6 mechanism. The solutions of the forward kinematic problem for the Stewart-6–6 mechanism is presented in Table IV. The data in the table correspond to the position of the moving platform. As seen in the table, the forward kinematic problem has 40 solutions. The first

https://doi.org/10.1017/S0263574716000862 Published online by Cambridge University Press

Table IV. Forward kinematic solutions of the Stewart-6–6 mechanism. The data correspond to the position of the center of the moving platform.

Solution	x (m)	y (m)	z (m)
1	0.1000	0.2000	0.3000
2	0.1000	0.2000	−0.3000
3	0.1337	−0.0021	0.3377
4	0.1337	−0.0021	−0.3377
5	0.0765	0.1351	0.2808
6	0.0765	0.1351	−0.2808
7	−0.0134	0.2633	0.2749
8	−0.0134	0.2633	−0.2749
9	−0.4346	1.3760	1.4281 i
10	−0.4346	1.3760	− 1.4281 i
11	0.3110	−0.6004	− 0.6116 i
12	0.3110	−0.6004	+ 0.6116 i
13	0.1423	0.9488	0.9157 i
14	0.1423	0.9488	− 0.9157 i
15	0.0867	−0.4781	0.1427 i
16	0.0867	−0.4781	− 0.1427 i
17	0.4101 − 0.2049 i	0.0163 + 0.0672 i	0.3308 + 0.3088 i
18	0.4101 + 0.2049 i	0.0163 − 0.0672 i	0.3308 − 0.3088 i
19	0.4101 − 0.2049 i	0.0163 + 0.0672 i	−0.3308 − 0.3088 i
20	0.4101 + 0.2049 i	0.0163 − 0.0672 i	−0.3308 + 0.3088 i
21	−0.0971 − 0.2393 i	−0.0019 + 0.1213 i	−0.4002 − 0.0093 i
22	−0.0971 + 0.2393 i	−0.0019 − 0.1213 i	−0.4002 + 0.0093 i
23	−0.0971 − 0.2393 i	−0.0019 + 0.1213 i	0.4002 + 0.0093 i
24	−0.0971 + 0.2393 i	−0.0019 − 0.1213 i	0.4002 − 0.0093 i
25	−0.0785 − 0.2322 i	0.3855 + 0.0607 i	0.3187 − 0.0809 i
26	−0.0785 + 0.2322 i	0.3855 − 0.0607 i	0.3187 + 0.0809 i
27	−0.0785 − 0.2322 i	0.3855 + 0.0607 i	−0.3187 + 0.0809 i
28	−0.0785+ 0.2322 i	0.3855 − 0.0607 i	−0.3187 − 0.0809 i
29	−0.1325 − 0.2100 i	−0.0569 + 0.0075 i	−0.3678 − 0.0215 i
30	−0.1325 + 0.2100 i	−0.0569 − 0.0075 i	−0.3678 + 0.0215 i
31	−0.1325 − 0.2100 i	−0.0569 + 0.0075 i	0.3678 + 0.0215 i
32	−0.1325 + 0.2100 i	−0.0569 − 0.0075 i	0.3678 − 0.0215 i
33	0.0418 − 0.2394 i	0.1506 − 0.0756 i	0.4735 + 0.0661 i
34	0.0418 + 0.2394 i	0.1506 + 0.0756 i	0.4735 − 0.0661 i
35	0.0418 − 0.2394 i	0.1506 − 0.0756 i	−0.4735 − 0.0661 i
36	0.0418 + 0.2394 i	0.1506 + 0.0756 i	−0.4735 + 0.0661 i
37	−0.1657 + 0.0092 i	0.1121 + 0.1519 i	−0.3349 + 0.0910 i
38	−0.1657 − 0.0092 i	0.1121 − 0.1519 i	−0.3349 − 0.0910 i
39	−0.1657 − 0.0092 i	0.1121 − 0.1519 i	0.3349 + 0.0910 i
40	−0.1657 + 0.0092 i	0.1121 + 0.1519 i	0.3349 − 0.0910 i

eight solutions are real, and the rest are complex. Therefore, beside the desired first solution, there are seven more possible poses for the moving platform which satisfy the forward kinematic equations. Schematic representations of the eight real solutions are shown in Fig. 11 with six legs connecting the moving platform to the fixed one. Isometric and top views of the mechanism are shown in the figure.

7. Applications of the Proposed Parallel Robots

With their 6-DOF moving platforms, these parallel robots are capable of moving in any direction or orientation within the space. They are ideal for various applications in aeronautics, automative industry, astronomy, machining, industrial testing, positioning, microscopy, semiconductor handling, biotechnology, and medical applications. In this section, two potential applications of the Wide-Open and 4-legged robots are briefly discussed.

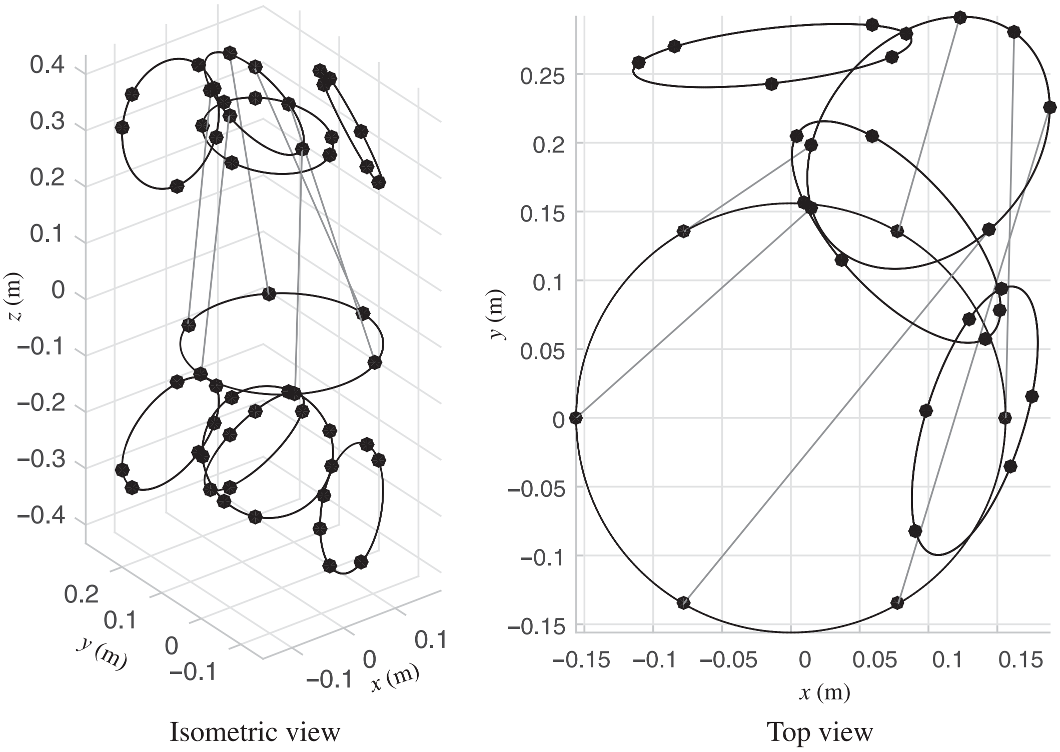

Fig. 11. Schematics of the real solutions of the forward kinematic problem of the Stewart-6–6 mechanism. Both isometric and top views of the solutions are illustrated. Six legs connect the moving platform to the fixed one.

7.1. The pole climbing robot

Pole climbing robots have many construction, service, and inspection applications in 3D tubular structures. The Wide-Open robot enjoys a frontally open structure, where it can easily embrace tubular structures. This notable advantage, makes it a perfect fit for pole climbing applications. The 6-DOF Wide-Open pole climber robot can travel along 3D tubular structures with bends, branches, and step changes in cross section. Figure 12 illustrates the application of the Wide-Open mechanism as a pole climber, where two grippers are provided for each platform.

The robot is able to do service works like welding operations, pipe testing in petrochemical plants, pipe/pole cleaning, light bulb changing, and cleaning in highways, etc.[39–43] It is also able to perform manipulation, repair, and maintenance tasks after reaching the target point on the structure. It can be used for construction and tall building maintenance, agricultural harvesting, highways and bridge maintenance, and shipyard production facilities.[44–48] There are also applications in industrial and hazardous environments, inspection of vertical and inclined pipes in nuclear power plants, wiring on high voltage power transmission towers, and inspection of high chimneys.[46]

7.2. Robotic assisted brain surgery

While all surgical procedures carry some risk, brain surgery carries extra risk because all the tissue of the organ is very delicate and of importance, making it an ideal candidate for robotic interventions. Using robotics for brain surgery provides the surgeon with many advantages. The most important advantages pertaining to neurosurgery are the ability to perform surgery on a smaller scale, increased accuracy and precision, access to small corridors, and the possibility of telesurgery.[49–51] The scale of neurosurgical procedures in the future is going to be so small that neurosurgeons will not be able to deliver them without the assistance of robots.[52]

Figure 13 illustrates the application of the redundantly actuated 4-legged robot in brain surgery, where high accuracy and large rotational workspace is needed. The redundantly actuated robot has dramatically much larger singularity-free workspace compared to its non-redundant 6-legged counterpart. The guide on the moving platform is able to precisely manipulate tools such as a probe,

Fig. 12. Illustration of the Wide-Open robot in a pole-climbing application. The robot is frontally open where it can easily embrace tubular objects. It can travel along tubular structures with bends, branches, and step changes in cross section. It is also able to perform manipulation, repair, and maintenance tasks after reaching the target point on the structure.

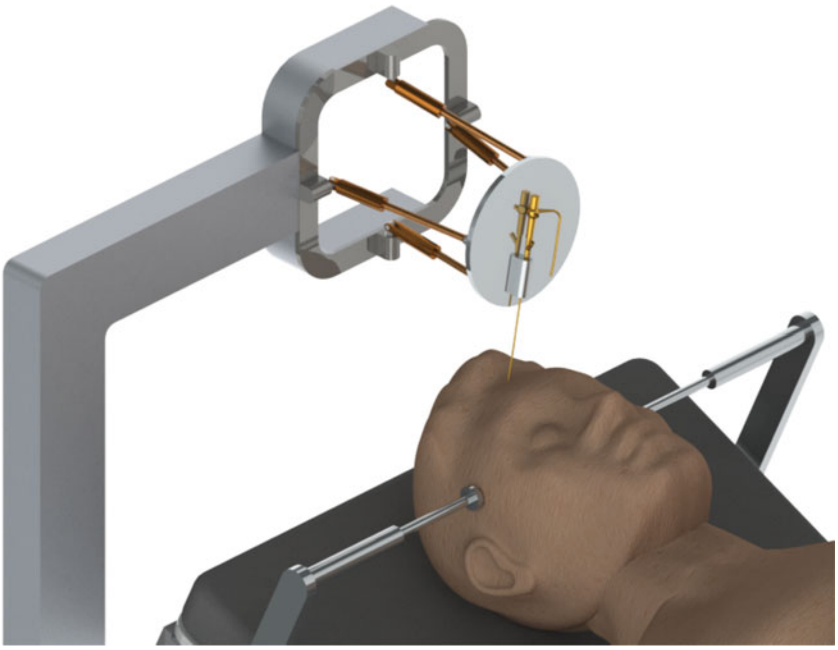

Fig. 13. Illustration of the redundantly actuated 4-legged robot with endoscope used for brain surgery. The robot is capable of delivering the ultra-precision resolution of sub-micron. The redundantly actuated robot has dramatically much larger singularity-free workspace compared to its non-redundant 6-legged counterpart.

endoscope, or retractor in six degrees of freedom. It can be used for instrument positioning and micropositioning, trajectory planning and precise needle insertion, motion and force scaling, and soft tissue cutting and destructing.

https://doi.org/10.1017/S0263574716000862 Published online by Cambridge University Press

Table V. Black square (■) indicates the best mechanism in term of different kinematic measures; manipulability, dexterity, sensitivity, reachable points, singularity, and forward kinematics.

Mechanism	red./Non-red.	Legs	Manip.	Dext.	Sens.	Reach.	Sing.	Fwd. Kin.
4L	Red.	4	■		■		■	■
WO	Non-red.	3				■		
3L	Non-red.	3						
Stewart (3–3)	Non-red.	6		■				
Stewart (3–6)	Non-red.	6						
Stewart (6–6)	Non-red.	6						

Table VI. Comparison of non-redundant mechanisms only. Black square (■) indicates the best mechanism in term of different kinematic measures; manipulability, dexterity, sensitivity, reachable points, singularity, and forward kinematics.

Mechanism	red./Non-red.	Legs	Manip.	Dext.	Sens.	Reach.	Sing.	Fwd. Kin.
WO	Non-red.	3				■		■
3L	Non-red.	3	■		■			■
Stewart (3–3)	Non-red.	6	■	■			■	
Stewart (3–6)	Non-red.	6						
Stewart (6–6)	Non-red.	6						

8. Conclusion

A group of 6-DOF UPS PMs were analyzed to study the effects of number of legs in their kinematic performance. From the design point of view, by replacing the passive universal joints in the Gough–Stewart platform with active joints, the number of legs could be reduced from 6 to 3 or 4. This makes the mechanism to be lighter, since the rotary actuators are resting on the fixed platform, which allows for higher accelerations to be achieved due to smaller inertial effects. The results indicate that the workspace of the PMs with reduced number of legs is much larger than that of the 6-legged Gough–Stewart platform. The performance comparisons are listed in Table V. Table V suggests that the redundancy in the 4L improves its capabilities to avoid kinematic singularities, to achieve higher manipulability, as well as lower sensitivity. Such advantages, in accompany with a high rigidity and a low inertia, make the 6-DOF 4-legged PM ideal for more challenging industrial applications in assembly, manufacturing, biomedical, and space technologies. In fact, it is suitable for a wide range of applications in flight simulators, surgical robots, rehabilitation systems, high precision positioning devices, motion generators, ultra-fast pick and place robots, entertainment systems, multi-axis machine tools, micro manipulators, and haptic instruments. Between the non-redundant mechanisms, right selection of number of legs depends on the priorities in kinematic measures in different applications, as seen in Table VI.

Acknowledgment

This work was supported in part by Iran National Science Foundation (INSF) under the grant number 91002447.

References

1. F. Gao, W. Li, X. Zhao, Z. Jin and H. Zhao, "New kinematic structures for 2-, 3-, 4-, and 5-dof parallel manipulator designs," *Mech. Mach. Theory* **37**(11), 1395–1411 (2002).
2. V. E. Gough and S. G. Whitehall, "Universal Tyre Test Machine," *Proceedings of the 9th International Technical Congress FISITA*, Birmingham, England (1962) pp. 117–137.
3. D. Stewart, "A platform with six degrees of freedom," *Proc. Inst. Mech. Eng.* **180**, 371–386 (1965).
4. Y. Patel and P. M. George, "Parallel manipulators applications–a survey," *Mod. Mech. Eng.* **2**(03), 57–64 (2012).
5. C. Gosselin and J. Angeles, "Singularity analysis of closed-loop kinematic chains," *IEEE Trans. Rob. Autom.* **6**(3), 281–290 (1990).

6. C. Gosselin and L.-T. Schreiber, "Kinematically redundant spatial parallel mechanisms for singularity avoidance and large orientational workspace," *IEEE Trans. Robot.* **32**(2), 286–300 (2016).
7. W. Shang and S. Cong, "Robust nonlinear control of a planar 2-dof parallel manipulator with redundant actuation," *Robot. Comput.-Integr. Manuf.* **30**(6), 597–604 (2014).
8. J. Wu, T. Li, J. Wang and L. Wang, "Stiffness and natural frequency of a 3-dof parallel manipulator with consideration of additional leg candidates," *Robot. Auton. Syst.* **61**(8), 868–875 (2013).
9. X.-M. Niu, G.-Q. Gao, X.-J. Liu and Z.-D. Bao, "Dynamics and control of a novel 3-dof parallel manipulator with actuation redundancy," *Int. J. Autom. Comput.* **10**(6), 552–562 (2013).
10. A. Müller, "Internal preload control of redundantly actuated parallel manipulators - its application to backlash avoiding control," *IEEE Trans. Rob.* **21**(4), 668–677 (2005).
11. B.-J. Yi, D. Cox and D. Tesar, "Analysis and Design Criteria for a Redundantly Actuated 4-Legged Six Degree-of-Freedom Parallel Manipulator," *Proceedings of the IEEE International Conference on Robotics and Automation, ICRA*, vol. 4, Seoul, South Korea, IEEE (2001) pp. 3286–3293.
12. T. Ropponen and Y. Nakamura, "Singularity-Free Parameterization and Performance Analysis of Actuation Redundancy," *Proceedings of the IEEE International Conference on Robotics and Automation*, vol. 2, Cincinnati, Ohio, USA, (1990) pp. 806–811.
13. D. Wang, R. Fan and W. Chen, "Performance enhancement of a three-degree-of-freedom parallel tool head via actuation redundancy," *Mechanism and Machine Theory* **71**, 142–162 (2014).
14. S. Shayya, S. Krut, O. Company, C. Baradat and F. Pierrot, "A Novel 4 dofs (3t-1r) Parallel Manipulator with Actuation Redundancy–Workspace Analysis," In MeTrApp'2013: 2nd Conference on Mechanisms, Transmissions and Applications, vol. 17, no. Mechanisms and Machine Science (Bilbao, Spain, October 2–4, 2013), pp. 317–324.
15. Y. Zhao and F. Gao, "The joint velocity, torque, and power capability evaluation of a redundant parallel manipulator," *Robotica* **29**(03), 483–493 (2011).
16. B.-J. Yi, R. A. Freeman and D. Tesar, "Open-Loop Stiffness Control of Overconstrained MechanismsRrobotic Linkage Systems," *Proceedings of the IEEE International Conference on Robotics and Automation*, vol. 3, Scottsdale, Arizona, USA (1989) pp. 1340–1345.
17. J. Wang and C. M. Gosselin, "Kinematic analysis and design of kinematically redundant parallel mechanisms," *J. Mech. Des. Trans. ASME* **126**(1), 109–118 (2004).
18. J. Kotlarski, B. Heimann and T. Ortmaier, "Influence of kinematic redundancy on the singularity-free workspace of parallel kinematic machines," *Frontiers Mech. Eng.* **7**(2), 120–134 (2012).
19. L. Beji and M. Pascal, "Kinematics and the full minimal dynamic model of a 6-dof parallel robot manipulator," *Nonlinear Dyn.* **18**, 339–356 (1999).
20. M. H. Abedinnasab and G. R. Vossoughi, "Analysis of a 6-dof redundantly actuated 4-legged parallel mechanism," *Nonlinear Dyn.* **58**(4), 611–622 (2009).
21. Mohammad H. Abedinnasab, Yong-Jin Yoon and Hassan Zohoor (2012). "Exploiting Higher Kinematic Performance - Using a 4-Legged Redundant PM Rather than Gough-Stewart Platforms," in *Serial and Parallel Robot Manipulators - Kinematics, Dynamics, Control and Optimization*, Dr. Serdar Kucuk (Ed.), InTech, DOI: 10.5772/32141.
22. O. Aghababai, Design, Kinematic and Dynamic Analysis and Optimization of a 6 DOF Redundantly Actuated Parallel Mechanism for Use in Haptic Systems*MSc Thesis* (Tehran, Iran: Sharif University of Technology, 2005).
23. J.-C. Faugère and D. Lazard, "Combinatorial classes of parallel manipulators," *Mech. Mach. Theory* **30**(6), 765–776 (1995).
24. C. W. Wampler, "Forward displacement analysis of general six-in-parallel sps (stewart) platform manipulators using soma coordinates," *Mech. Mach. Theory* **31**(3), 331–337 (1996).
25. J. Gallardo-Alvarado, "A simple method to solve the forward displacement analysis of the general six-legged parallel manipulator," *Robot. Comput.-Integrated Manuf.* **30**(1), 55–61 (2014).
26. X.-S. Gao, D. Lei, Q. Liao and G.-F. Zhang, "Generalized stewart-gough platforms and their direct kinematics," *IEEE Trans. Robot.* **21**(2), 141–151 (2005).
27. J. Gallardo-Alvarado, R. Rodríguez-Castro and M. N. Islam, "Analytical solution of the forward position analysis of parallel manipulators that generate 3-rs structures," *Adv. Robot.* **22**(2–3), 215–234 (2008).
28. Y. Zhao, J. Liu and Z. Huang, "A force analysis of a 3-rps parallel mechanism by using screw theory," *Robotica* **29**(07), 959–965 (2011).
29. J. Gallardo-Alvarado, H. Orozco-Mendoza and J. M. Rico-Martínez, "A novel five-degrees-of-freedom decoupled robot," *Robotica* **28**(6), 909–917 (2010).
30. J. Gallardo-Alvarado, J. M. Rico-Martínez and G. Alici, "Kinematics and singularity analyses of a 4-dof parallel manipulator using screw theory," *Mech. Mach. Theory* **41**(9), 1048–1061 (2006).
31. J. Zhao, B. Li, X. Yang and H. Yu, "Geometrical method to determine the reciprocal screws and applications to parallel manipulators," *Robotica* **27**(06), 929–940 (2009).
32. L.-W. Tsai, *Robot Analysis: The Mechanics of Serial and Parallel Manipulators* (Wiley, New York, New York, USA, 1999).
33. L.-W. Tsai, "The jacobian analysis of a parallel manipulator using reciprocal screws," **In:** *Advances in Robot Kinematics: Analysis and Control* (J. Lenarcic and M. L. Husty, eds.) (Kluwer Academic, 1998), 327–336.
34. I. Mansouri and M. Ouali, "The power manipulability a new homogeneous performance index of robot manipulators," *Rob. Comput. Integr. Manuf.* **27**(2), 434–449 (2011).

35. J. Angeles and C. S. Lopez-Cajun, "Kinematic isotropy and the conditioning index of serial robotic manipulators," *Int. J. Rob. Res.* **11**(6), 560–571 (1992).
36. C. M. Gosselin, "The optimum design of robotic manipulators using dexterity indices," *Rob. Autom. Syst.* **9**(4), 213–226 (1992).
37. P. Cardou, S. Bouchard and C. Gosselin, "Kinematic-sensitivity indices for dimensionally nonhomogeneous jacobian matrices," *IEEE Trans. Robot.* **26**(1), 166–173 (2010).
38. C. Gosselin and J. Angeles, "Global performance index for the kinematic optimization of robotic manipulators," *J. Mech. Transm. Autom. Des.* **113**(3), 220–226 (1991).
39. M. Tavakoli, M. Zakerzadeh, G. Vossoughi and S. Bagheri, "A hybrid pole climbing and manipulating robot with minimum dofs for construction and service applications," *Ind. Robot: Int. J.* **32**(2), 171–178 (2005).
40. M. Tavakoli, A. Marjovi, L. Marques and A. T. De Almeida, "3dclimber: A Climbing Robot for Inspection of 3d Human Made Structures," *Proceedings of the IEEE/RSJ International Conference on Intelligent Robots and Systems, IROS*, Nice, France (2008) pp. 4130–4135.
41. M. Tavakoli, L. Marques and A. T. de Almeida, "Development of an industrial pipeline inspection robot," *Ind. Robot: Int. J.* **37**(3), 309–322 (2010).
42. M. Tavakoli, P. Lopes, L. Sgrigna and C. Viegas, "Motion control of an omnidirectional climbing robot based on dead reckoning method," *Mechatronics* **30**, 94–106 (2015).
43. J. E. Clark, J. G. Cham, S. Bailey, E. M. Froehlich, P. K. Nahata, R. J. Full, M. R. Cutkosky, "Biomimetic Design and Fabrication of a Hexapedal Running Robot," *Proceedings of the IEEE International Conference on Robotics and Automation, ICRA*, vol. 4, Seoul, South Korea (2001) pp. 3643–3649.
44. S. Kim, M. Spenko, S. Trujillo, B. Heyneman, D. Santos and M. R. Cutkosky, "Smooth vertical surface climbing with directional adhesion," *IEEE Trans. Robot.* **24**(1), 65–74 (2008).
45. M. Spenko, G. Haynes, J. Saunders, M. Cutkosky, A. Rizzi, R. Full and D. Koditschek, "Biologically inspired climbing with a hexapedal robot," *J. Field Robot.* **25**(4–5) (2008) 223–242.
46. A. Baghani, M. N. Ahmadabadi and A. Harati, "Kinematics Modeling of a Wheel-Based Pole Climbing Robot (ut-pcr)," *Proceedings of the 2005 IEEE International Conference on Robotics and Automation, ICRA*, Barcelona, Spain (2005), pp. 2099–2104.
47. M. Almonacid, R. J. Saltarén, R. Aracil and O. Reinoso, "Motion planning of a climbing parallel robot," *IEEE Trans. Robot. Autom.* **19**(3), 485–489 (2003).
48. R. Aracil, R. Saltarén and O. Reinoso, "Parallel robots for autonomous climbing along tubular structures," *Robot. Auton. Syst.* **42**(2), 125–134 (2003).
49. L. Zamorano, Q. Li, S. Jain and G. Kaur, "Robotics in neurosurgery: State of the art and future technological challenges," *Int. J. Med. Robot.* **1**(1), 7–22 (2004).
50. P. B. McBeth, D. F. Louw, P. R. Rizun and G. R. Sutherland, "Robotics in neurosurgery," *Am. J. Surg.* **188**(4), 68–75 (2004).
51. N. Nathoo, M. C. Çavusoglu, M. A. Vogelbaum and G. H. Barnett, "In touch with robotics: neurosurgery for the future," *Neurosurgery* **56**(3), 421–433 (2005).
52. M. S. Eljamel, *Robotic Applications in Neurosurgery* (INTECH Open Access Publisher, Rijeka, Croatia, 2008).

https://doi.org/10.1017/S0263574716000862 Published online by Cambridge University Press